



Article (refereed) - postprint

Blaker, A.T.; Hirschi, J.J.- M.; McCarthy, G.; Sinha, B.; Taws, S.; Marsh, R.; de Cuevas, B.A.; Alderson, S.G.; Coward, A.C.. 2015 Historical analogues of the recent extreme minima observed in the Atlantic meridional overturning circulation at 26°N. *Climate Dynamics*, 44 (1-2). 457-473. [10.1007/s00382-014-2274-6](https://doi.org/10.1007/s00382-014-2274-6)

© Springer Science+Business Media B.V. 2015

This version available at <http://nora.nerc.ac.uk/507439/>

NERC has developed NORA to enable users to access research outputs wholly or partially funded by NERC. Copyright and other rights for material on this site are retained by the rights owners. Users should read the terms and conditions of use of this material at <http://nora.nerc.ac.uk/policies.html#access>

This document is the author's final manuscript version of the journal article, incorporating any revisions agreed during the peer review process. Some differences between this and the publisher's version remain. You are advised to consult the publisher's version if you wish to cite from this article.

The final publication is available at link.springer.com

Contact NOC NORA team at
publications@noc.soton.ac.uk

1 **Historical analogues of the recent extreme minima observed in**
2 **the Atlantic meridional overturning circulation at 26°N**

3 **Adam T. Blaker · Joël J-M. Hirschi · Gerard**
4 **McCarthy · Bablu Sinha · Sarah Taws · Robert**
5 **Marsh · Andrew Coward · Beverly de Cuevas**

6
7 Received: date / Accepted: date

8 **Abstract** Observations of the Atlantic meridional overturning circulation (AMOC) by the
9 RAPID 26°N array show a pronounced minimum in the northward transport over the winter
10 of 2009/10, substantially lower than any observed since the initial deployment in April 2004.
11 It was followed by a second minimum in the winter of 2010/2011. We demonstrate that
12 ocean models forced with observed surface fluxes reproduce the observed minima.

13 Examining output from five ocean model simulations we identify several historical
14 events which exhibit similar characteristics to those observed in the winter of 2009/10,
15 including instances of individual events, and two clear examples of pairs of events which
16 happened in consecutive years, one in 1969/70 and another in 1978/79. In all cases the ab-
17 solute minimum, associated with a short, sharp reduction in the Ekman component, occurs
18 in winter. AMOC anomalies are coherent between the Equator and 50°N and in some cases
19 propagation attributable to the poleward movement of the anomaly in the wind field is ob-
20 served. We also observe a low frequency (decadal) mode of variability in the anomalies,
21 associated with the North Atlantic Oscillation (NAO).

22 Where pairs of events have occurred in consecutive years we find that atmospheric con-
23 ditions during the first winter correspond to a strongly negative Arctic Oscillation (AO)
24 index. Atmospheric conditions during the second winter are indicative of a more regional
25 negative NAO phase, and we suggest that this persistence is linked to re-emergence of sea
26 surface temperature anomalies in the North Atlantic for the events of 1969/70 and 2009/10.
27 The events of 1978/79 do not exhibit re-emergence, indicating that the atmospheric memory
28 for this pair of events originates elsewhere. Observation of AO patterns associated with cold
29 winters over northwest Europe, may be indicative for the occurrence of a second extreme
30 winter over northwest Europe.

31 **Keywords** AMOC · minimum · events · RAPID · model · observations · SST anomalies ·
32 re-emergence

Adam Blaker
National Oceanography Centre, Southampton, SO14 3ZH
E-mail: atb299@noc.ac.uk

1 Introduction

The Atlantic meridional overturning circulation (AMOC) is part of the global ocean conveyor which transports warm and saline surface waters to the North Atlantic (Broecker, 1987; Dickson and Brown, 1994; Kuhlbrodt et al, 2007). On their journey towards the Nordic seas these surface waters gradually become denser as they release heat to the atmosphere. Eventually, the increasing density leads to the sinking of the water masses and they are returned southward as cold and dense North Atlantic deep water. In the subtropical North Atlantic the surface and deep branches of the AMOC result in a maximum net northward heat transport of around 1.3 PW (Ganachaud and Wunsch, 2000; Lumpkin and Speer, 2007; Johns et al, 2011). The AMOC has been identified as a key ocean mechanism which contributes to the comparatively mild European climate. A large fraction of the heat released to the atmosphere by the AMOC is carried eastward towards Europe by the predominant westerly winds, leading to warmer temperatures in northwestern Europe than at similar latitudes in western Canada (Rhines and Häkkinen, 2003; Broecker, 1987; Sinha et al, 2012). The potential importance of the AMOC to the climate of the North Atlantic and Europe was a key motivation for the deployment of a transatlantic mooring array at 26.5°N , known as the RAPID-WATCH/MOCHA/WBTS array (hereafter referred to as the 26°N array) (Rayner et al, 2011).

Observation- and model based studies have shown the AMOC transport at 26.5°N to exhibit substantial variability on short timescales (Cunningham et al, 2007; Kanzow et al, 2009, 2010; Hirschi and Marotzke, 2007; Baehr et al, 2007, 2009; Balan Sarojini et al, 2011; McCarthy et al, 2012). The observed intra-annual peak-to-peak range of the AMOC, computed using daily means, can be as large as 30 Sv (Cunningham et al, 2007). Between April 2004 and April 2009, the AMOC transport at 26.5°N has a mean of 18.5 Sv, with a standard deviation of 4.7 Sv, when computed using 5 day means. The origin of the observed AMOC variability is only partly understood. Some variability, such as the observed seasonality of the AMOC and interannual variability seen in numerical models, can be linked to the seasonal variability in the wind stress curl along the African coast (Kanzow et al, 2010; Chidichimo et al, 2010; Sinha et al, 2013).

Observations from the 26°N array revealed a recent strong short-term reduction in the strength of the AMOC (McCarthy et al, 2012). The event lasted for 3-4 months over the late winter and early spring of 2009/2010, and resulted in the April-March annual average for that year reducing to 12.8 Sv, 30% lower than the mean for the previous 5 years. This is the first such event to occur in the 7 year long record from the 26°N array, and it is not known whether events of this kind have occurred in the past. It was followed the year after by a similarly anomalous minimum, raising the question of whether the two events were linked, or whether they occurred consecutively by coincidence. To try and address this question we employ ocean models forced with historical observations of surface fluxes. We examine the characteristics of anomalously low AMOC events in five $1/4^{\circ}$ model integrations which all cover the period 1958-2001 and two further model integrations, one at $1/4^{\circ}$ and one at $1/12^{\circ}$, which cover the period between 2001 and 2011.

Outline The remainder of this article is organized as follows. Section 2 describes the ensemble of models used. Our analysis is presented in section 3. Finally, we summarise our findings in section 4.

Table 1 This table shows the model configurations used. All are ORCA025 ($1/4^\circ$) except ORCA12, which is $1/12^\circ$. The ORCA12 simulation includes a minor code change in 1989, and a change in surface forcing in 2007 in order to extend out to 2010.

Run ID	Code version	Ice model	Levels	Forcing	Period
N102	v2.3	LIM2	64	DFS3	1958-2001
N112	v2.3	LIM2	64	DFS3	1958-2001
N200	v2.3	LIM2	64	DFS4.1	1958-2001
N206	v3.2	LIM2	75	CORE2	1958-2007
N300	v3.0	LIM3	64	DFS3	1958-2001
VN206	v3.2	LIM2	75	ERA Interim	1989-2011
ORCA12	v3.2/v3.3.1	LIM2	75	DFS4.1/DFS5.1.1	1978-2010

77 2 Method

78 2.1 Observation based datasets

79 For the analysis presented here we use the following observation based datasets.

80 The AMOC measured by the 26°N array is the sum of the transport measured through
 81 the Florida Straits, the geostrophic component derived from measurements of the den-
 82 sity difference between the eastern and western boundaries, Ekman transport derived from
 83 CCMP/Quikscat winds, and a compensation term which ensures that there is no net trans-
 84 port through the section (Rayner et al, 2011). Ocean models suggest that the sum of these
 85 is a close approximation to the true AMOC which one could compute if the northward ve-
 86 locity at all points through the section were known (Hirschi and Marotzke, 2007; Hirschi
 87 et al, 2003). Data from the 26°N array (<http://www.rapid.ac.uk>) are provided at 12
 88 hourly resolution with a 10 day low pass filter applied. Observations of all component time
 89 series are available from April 2004 to present. For our analysis we compute 5 day aver-
 90 ages to facilitate comparison with the model simulations, for which output is stored as 5 day
 91 averages.

92 To explore the geographical nature of the events we use monthly mean sea level pres-
 93 sure and surface air temperature data from the NCEP/NCAR reanalysis dataset (Kalnay
 94 et al, 1996). We relate the events identified to the monthly indices of the North Atlantic
 95 and Arctic Oscillations following Hurrell (1995) (NCAR, 2012a,b). To examine the mech-
 96 anism of re-emergence we make use of SST data from the NOAA optimal interpolation
 97 dataset (Reynolds et al, 2002) <http://www.esrl.noaa.gov/psd/> and also of the EN-
 98 ACT (EN3) reanalysis from the UK Met Office (Ingleby and Huddleston, 2007) <http://www.metoffice.gov.uk/hadobs/en3/>.

100 2.2 Model description and runs

101 We use a total of seven NEMO (Nucleus for European Modelling of the Ocean) ORCA
 102 (Madec, 2008) model integrations, most of which were set up in the DRAKKAR project
 103 (DRAKKAR Group, 2007; Barnier et al, 2006; Madec, 2008), and one run from the RAPID-
 104 WATCH VALOR project. Table 1 details the runs.

105 Five simulations start from 1958, and form the ensemble which we will analyse in this
 106 paper. Aspects of the AMOC in some of these runs have been published previously (Grist
 107 et al, 2010, 2012; Blaker et al, 2012; Hirschi et al, 2013; Ducheux et al, 2014b). All of these
 108 simulations are on the ORCA025 grid, for which horizontal resolution is nominally $1/4^\circ$.

109 South of 20°N the model grid is isotropic Mercator, and north of 20°N the grid becomes
110 quasi-isotropic bipolar, with poles located in Canada and Siberia to avoid numerical insta-
111 bility associated with convergence of the meridians at the geographic North Pole. At the
112 Equator the resolution is approximately 27.75 km, becoming finer at higher latitudes such
113 that at 60°N/S it becomes 13.8 km. The models in the ensemble include both 64 and 75
114 vertical levels with a grid spacing increasing from 6 m near the surface (1 m for the 75 level
115 runs) to 250 m at 5500 m. Bottom topography is represented as partial steps and bathymetry
116 is derived from ETOPO2 (U.S. Department of Commerce, 2006). To prevent excessive drifts
117 in global salinity due to deficiencies in the fresh water forcing, sea surface salinity is relaxed
118 towards climatology with a piston velocity of 33.33 mm/day/psu. Sea ice is represented by
119 the Louvain-la-Neuve Ice Model version 2 (LIM2) sea-ice model (Timmerman et al, 2005),
120 and version 3 of the same for one of the runs.

121 Climatological initial conditions for temperature and salinity were taken in January from
122 PHC2.1 (Steele et al, 2001) at high latitudes, MEDATLAS (Jourdan et al, 1998) in the
123 Mediterranean, and Levitus et al (1998) elsewhere. These initial conditions were applied to
124 all runs with the exception of N112, which started from the final state of N102, and VN206,
125 which started from the final state of N206. Starting from rest the models simulate the period
126 indicated in the right hand column of table 1, with surface forcing comprising of 6-hourly
127 mean momentum fields, daily mean radiation fields and monthly mean precipitation fields
128 supplied by the DFS3, DFS4.1 and CORE2 datasets (Brodeau et al, 2010; Large and Yeager,
129 2004, 2008) and linearly interpolated from the time mean fields by the model. Model output
130 is stored as 5-day averages, although for disk storage considerations, we have only retained
131 monthly mean values for some of the older datasets.

132 One $1/4^{\circ}$ run, VN206, is forced by the ERA Interim dataset (Dee et al, 2011) and extends
133 to March 2011. We also examine the output of a recently completed ORCA12 ($1/12^{\circ}$) run,
134 which again uses the NEMO ORCA code, but is now eddy resolving for much of the global
135 ocean.

136 The ensemble of model integrations we have compiled here are all closely related. They
137 are runs of the same model with minor/moderate variations in the code version, applied sur-
138 face forcing, ice model used and initial conditions, and all reproduce plausible ocean states.
139 For each of the model runs we compute the AMOC and component parts equivalent to those
140 which are measured and used to construct the time series at 26.5°N . Florida Straits transport
141 in the model integrations is computed as the integral of the meridional velocity through the
142 Florida Straits. The Upper Mid Ocean component is computed by integrating the east-west
143 density difference derived geostrophic transport across the basin. Ekman transport is com-
144 puted using the surface wind stress. A uniform compensation velocity which ensures no net
145 volume transport through the section is applied. Details of the component decomposition
146 method are provided in Appendix A.

147 3 AMOC analysis

148 3.1 Comparison with observations

149 In order to establish whether the NEMO ORCA model is able to capture the features of
150 the events seen in the observations we first examine model output from runs VN206 and
151 ORCA12 (Figure 1; see Table 1 for details of these runs). These are the only experiments
152 which cover the recently observed minima. The transport and components from VN206 are
153 shown in Figure 1 a), and for ORCA12 in Figure 1 b). The components measured by the

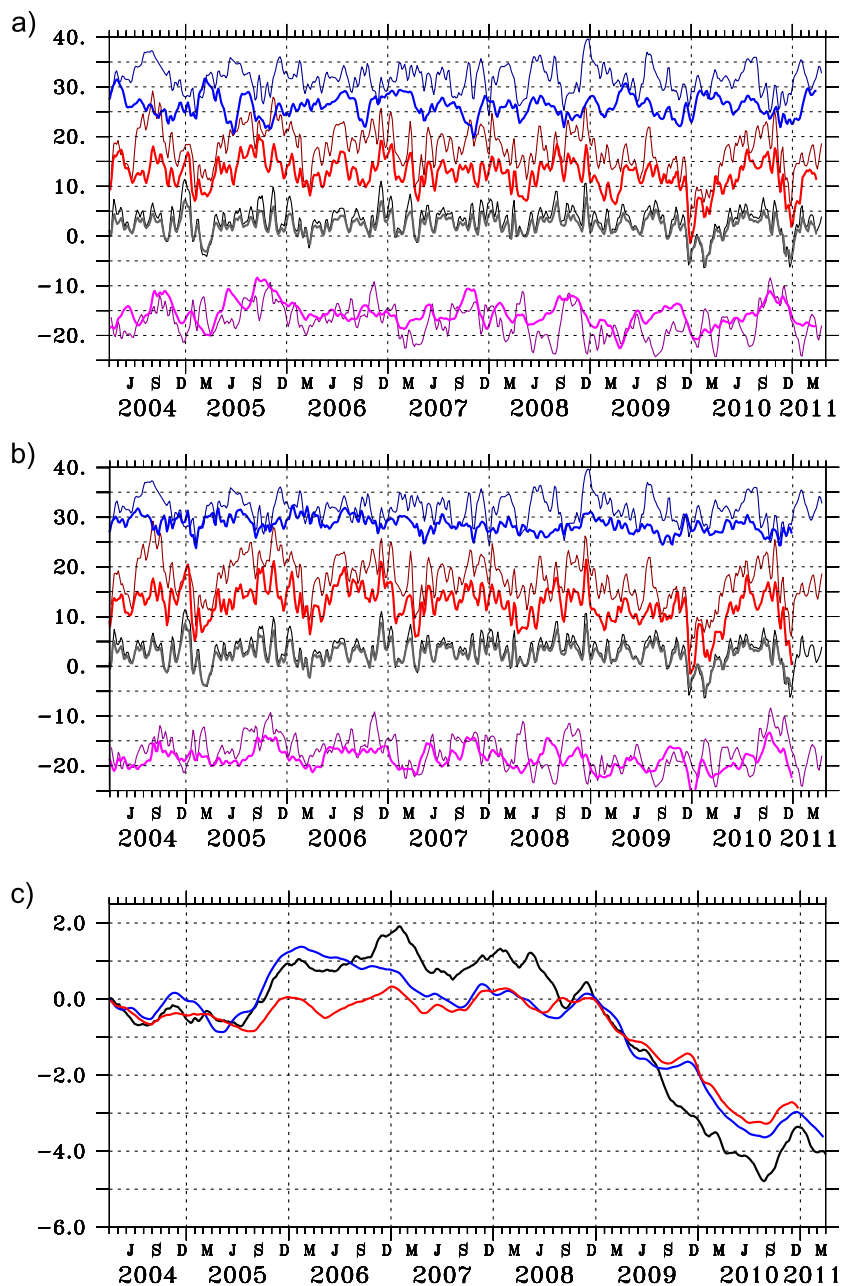


Fig. 1 Comparison of the component time series of the Atlantic MOC between the simulations (a) VN206, and b) ORCA12) and the RAPID observations. In the top two panels the model time series are shown in bold lines, and the observations are shown in thin lines: the Florida Straits transport (blue), Ekman (black), upper mid ocean (UMO) transport (magenta), and total AMOC (red). A slightly darker shade of the same colour is used for the observations to aid identification where lines overlay. Units are Sverdrups ($1\text{ Sv} = 1 \times 10^6 \text{ m}^3 \text{ s}^{-1}$) and data are smoothed with a 15 day Parzen filter. c) shows the accumulated transport anomaly for the UMO component of the transport for the RAPID observations (black), VN206 (blue) and ORCA12 (red). Transport anomalies are defined to be the UMO component with the time average for the period April 2004 to December 2008 subtracted. The anomalous transports are then accumulated over time. Units are Sverdrup years.

154 mooring array at 26.5°N are shown in each plot as thin, slightly darker lines of the same
155 shade. The mean, standard deviation and correlation between the modelled and observed
156 time series are presented in Table 2. As expected, the Ekman component is well represented
157 in the simulations (correlations of 0.88 and 0.84) although both have a weaker mean and
158 standard deviation than reported from observations. Both simulations exhibit weaker Florida
159 Straits (FS) transports than observed. The mean FS transport in VN206 is 5.5 Sv (17%)
160 weaker than observed. ORCA12 captures the mean transport better, but underestimates the
161 variability. It is interesting to note that FS transport variability is even lower in ORCA12 than
162 in VN206. The variability of the FS transport (and of any other western boundary current)
163 depends on the choice of the lateral boundary condition. Using no-slip conditions has been
164 shown to destabilise western boundary currents leading to more mesoscale ocean eddies and
165 variability close to lateral boundaries (Quarty et al, 2013). This behaviour has also been
166 observed in a suite of ORCA12 simulations conducted in the framework of the DRAKKAR
167 project (Deshayes et al, 2013) where the variability of western boundary currents is found
168 to be systematically higher when using partial slip conditions. Correlations between the
169 modelled and observed FS transport are low (0.22 and 0.35), indicating that a large fraction
170 of the FS variability cannot directly be attributed to the surface forcing. The correlation
171 between the FS transport time series from the two model runs is also low (0.35), which
172 suggests that the FS transport variability is dominated by internal variability. Both models
173 capture the mean upper mid ocean (UMO) transport. They also appear to capture the low
174 frequency (seasonal and longer) variability of the observed UMO time series, but fail to
175 capture the higher frequency variability (Figure 1). This behaviour may arise because the
176 low frequency variability of the UMO transport at 26.5°N is well approximated by the
177 surface forced Sverdrup transport (Duchez et al, 2014b). The seasonal cycle of the total
178 AMOC and the UMO component are well represented in the models, with respect to both
179 the timing and amplitude (Duchez et al, 2014a).

180 The extreme events which occur during the winters of 09/10 and 10/11 both reach their
181 peak in late December. Taking a 30 day average of the observations and subtracting from
182 the time mean observational values, the anomalous Ekman component contributes 52% of
183 the first AMOC minimum and around 80% of the second. Both simulations (ORCA12 and
184 VN206) agree well with the observations for the first event (55% and 51% respectively).
185 For the second event the Ekman component contributes 50% (ORCA12) and 46% (VN206)
186 for the two simulations. An observed negative anomaly in the UMO transport, which be-
187 gan early in 2009 and was associated with a partial shift of the circulation from the deep
188 overturning to the upper gyre circulation, was found to contribute significantly to the min-
189 imum event of 2009/10 (McCarthy et al, 2012). To establish how well the UMO anomaly
190 is represented by the simulations we compute the accumulated UMO transport anomaly in
191 the manner of Bryden et al (2014) (Figure 1c). The accumulated transport anomaly is the
192 cumulative summation of UMO anomalies from April 2004 (the start of the observational
193 period) to the end of the simulations/observations. Presenting the anomalies in this way em-
194 phasises anomalies of a consistent sign, whilst reducing the visual effect of differences in
195 the timing of short term variability between the simulations and observations. It indicates
196 that the models also capture around two thirds of the anomalous transport associated with
197 the UMO.

198 These figures indicate that to first order the extreme minima in the AMOC are, consistent
199 with Zhao and Johns (2014), atmospherically forced processes, which NEMO is able to
200 represent.

Table 2 This table shows the mean and standard deviation (brackets) for each time series shown in Figure 1. Correlations between each model and the observations, based on 5 day mean values, are given in italics. Shown in brackets in the right hand column is the correlation of each time series between the two models.

	Obs	VN206	ORCA12	
AMOC	17.47 (4.78)	12.37 (3.26)	12.57 (3.72)	
		<i>0.74</i>	<i>0.73</i>	(0.83)
Florida Strait	31.56 (3.02)	26.03 (2.15)	28.57 (1.56)	
		<i>0.22</i>	<i>0.35</i>	(0.35)
Ekman	3.19 (3.32)	2.04 (2.08)	2.56 (2.26)	
		<i>0.88</i>	<i>0.84</i>	(0.93)
UMO	-17.22 (3.47)	-15.66 (2.49)	-18.44 (2.07)	
		<i>0.47</i>	<i>0.43</i>	(0.65)

201 3.2 Historical analogues

202 The array measurements only extend back as far as 2004, but our ocean models are typi-
 203 cally forced with atmospheric observations from as early as 1958. Since we have confidence
 204 that NEMO ORCA is able to reproduce events such as the ones observed in 2009/10 given
 205 only surface forcing, we can examine the time series of the AMOC from our ensemble of
 206 historical model runs for examples of similar events.

207 We construct a composite of the AMOC anomalies (Ψ') from the five eddy permit-
 208 ting hindcasts that span the time period 1958-2001 by removing the linear trend from each
 209 ensemble member and then removing the seasonal cycle. The AMOC anomalies are then
 210 averaged to produce the ensemble mean, Figure 2). This composite reveals several strongly
 211 negative events, some substantially in excess of 2 standard deviations from the mean. There
 212 is a strong negative event in 1962/63, one in 1980/81 and another in 1983/84. There is also
 213 a minimum in 1986/87 with a duration of 3-4 months. We can also identify two pairs of
 214 events, one pair in 1968/69 and 1969/70, and another pair in 1977/78 and 1978/79. One fur-
 215 ther example in the time series which may also be a weaker analogue of the 2009/10 event
 216 occurs during 1996/97 and 1997/98. The event in the winter of 1996/97 occurs slightly later
 217 (around March) than other events in the time series (typically January-February). It coin-
 218 cides with an anomalously strong northward Ekman transport anomaly in February, which
 219 we suggest is likely to have reduced the impact and altered the timing of the negative event.

220 From the observed events we know that a large fraction of the minimum arises from
 221 the Ekman component (Figure 1, and also McCarthy et al (2012)), and the high correlation
 222 between the Ekman component and the AMOC (0.87) can be seen in Figure 2 (a and d).
 223 It is worth noting that the ensemble spread for the Ekman component is very small, which
 224 is a reflection of the similarities among the forcing datasets and how strongly the Ekman
 225 component is controlled by the surface forcing. Whilst variability of the Ekman component
 226 is the largest single contributor, it does not explain all of the variability in the AMOC. The
 227 value of two standard deviations in the AMOC is 4 Sv. Two standard deviations of the Ek-
 228 man component alone is 2.7 Sv, whilst the variability associated with the other components
 229 combined is slightly higher than this at 2.95 Sv. However, we note that for months which
 230 exhibit a negative AMOC anomaly of greater than 2 standard deviations, we find that on
 231 average the Ekman component contributes 62% of the anomaly. Some interaction between
 232 the FS transport and the geostrophic transport can also be seen in Figure 2 (b and c), which
 233 have a correlation of -0.55. This is partly attributable to the inclusion of the FS compensa-
 234 tion in the UMO transport, and partly to variation in the path of the Gulf Stream, with some
 235 fraction of the transport occasionally passing to the east of the Bahamas instead of through

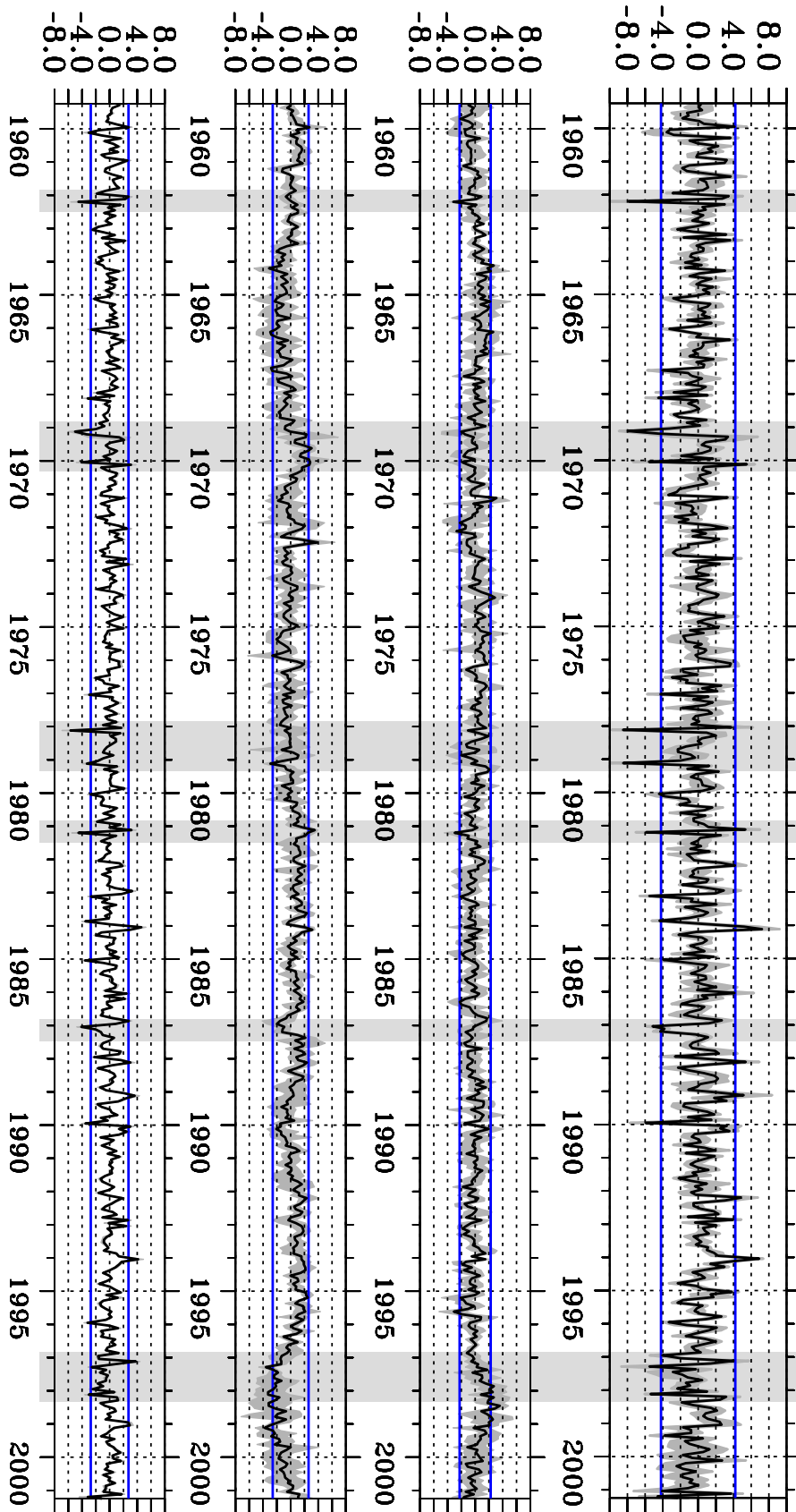


Fig. 2 Composite (monthly mean) of detrended time series with mean seasonal cycle removed for the years 1959-2001 from the 5 ORCA025 hindcasts. AMOC (Top), FST (upper middle), GEO (lower middle) and EKM (bottom). Blue lines denote ± 2 standard deviations for each component. Grey underlay denotes the ensemble spread for each month. Units are Sv. The events discussed in the text are indicated using vertical grey bars.

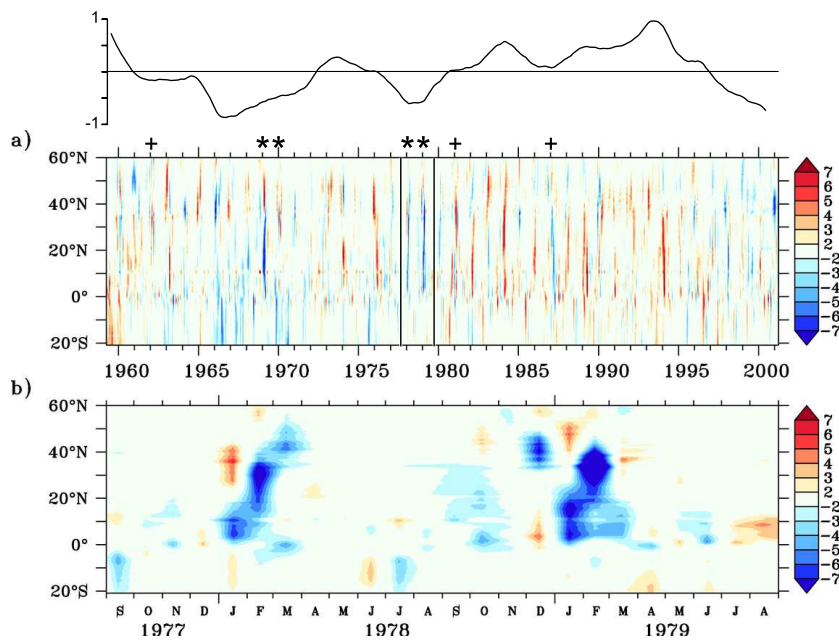


Fig. 3 Composite (monthly mean) of the AMOC with the mean and seasonal cycle removed as a function of latitude. a) time period from April 1959 through till March 2001, and b) expansion of time period from September 1977 through till August 1979. The line plot above a) is the meridional average of the transport anomaly presented in a). The events discussed in the text are indicated with * (pair events) and + (single events). Units are Sv.

236 the FS. This may be an artefact of the model resolution. The ensemble spread is large for
 237 the FS transport and the geostrophic transport, and this reflects the differences in timings of
 238 short timescale chaotic events (e.g. mesoscale ocean eddies, Gulf Stream meanders), which
 239 account for about 30% of the total AMOC variability (Hirschi et al, 2013).

240 The distribution of extreme AMOC events is asymmetric. There are only two positive
 241 anomalies stronger than 6 Sv, one in 1984 and one in 1994, both of which coincide with
 242 strong positive anomalies in the Ekman transport. In contrast there are 6 negative events
 243 which exceed 6 Sv. However, the time series is too short and there are insufficient events to
 244 say whether this is statistically significant.

245 3.3 Latitudinal characteristics

246 We compute the anomalies of the AMOC for the ensemble mean as a function of latitude and
 247 time (Figure 3), revealing that the anomalies in the AMOC are short (order 1-2 months) at all
 248 latitudes. It is also interesting to note that the anomalies, both of positive and negative sign,
 249 predominantly occur during the boreal winter months. This reflects the much greater vari-
 250 ability in northern hemisphere atmospheric circulation during the winter months, whilst the
 251 summers are more stable and therefore less likely to give rise to extreme anomalies. Anoma-
 252 lies are more frequent near the Equator and around 40°N where the Gulf Stream separates
 253 from the coast and becomes more zonal, and are typically confined to smaller latitudinal
 254 extents as would be expected for anomalies which arise due to the presence of strong eddy

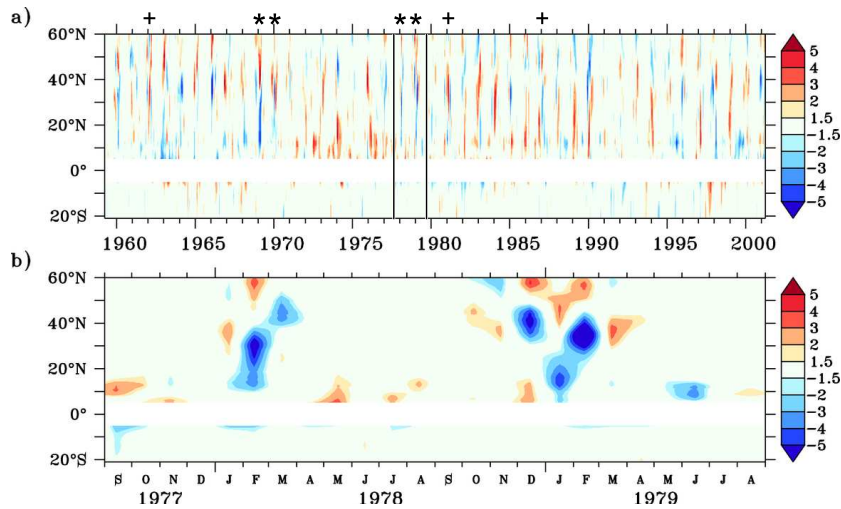


Fig. 4 Composite (monthly mean) of the Ekman component with the mean and seasonal cycle removed as a function of latitude. a) time period from April 1959 through till March 2001, and b) expansion of time period from September 1977 through till August 1979. The events discussed in the text are indicated with * (pair events) and + (single events). Units are Sv.

255 or wave activity. There are several anomalies which have a much greater latitudinal extent,
 256 from near the Equator to 50°N.

257 Expanding the time axis around a region of interest, such as the strong minima events
 258 observed during the winters of 1977/78 and 1978/79 (Figure 3b)) shows that many of the
 259 anomalies propagate poleward, covering 50° of latitude in 1-2 months. Anomalies start
 260 near the Equator in December/January and reach 40-50°N by March/April. The similarity
 261 between the Ekman component (Figure 4) and the AMOC (Figure 3) indicates that the
 262 propagation is a poleward shift of the Ekman anomaly caused by meridionally propagating
 263 anomalies in the mean surface wind field. This characteristic is not specifically associated
 264 with the extreme anomalies. It also occurs in other years, typically during the winter months.

265 To further examine the northward propagation of the AMOC anomalies we examine
 266 in detail the anomalous Ekman transport from recent winter 2010/11. Figure 5 illustrates
 267 how the zonal wind stress anomalies over the North Atlantic change over time by step-
 268 ping through 35 days which cover the northward propagation of this anomaly. A positive
 269 anomaly, corresponding to a weakening of the easterly winds, forms and begins to strengthen
 270 over the western half of the Atlantic basin between 15°N and 35°N in mid December. Posi-
 271 tive (i.e. westerly) anomalies north of the Equator result in an anomalous southward Ekman
 272 transport. The positive anomaly intensifies over the next 10 days and begins to propagate
 273 north and spread across the basin. By early January the anomaly is located between 26°N
 274 and 45°N, and by mid January it begins to weaken, the southernmost part of the anomaly
 275 weakening first. The AMOC anomaly associated with this anomalous wind stress can exceed
 276 -12 Sv for a 5 day mean.

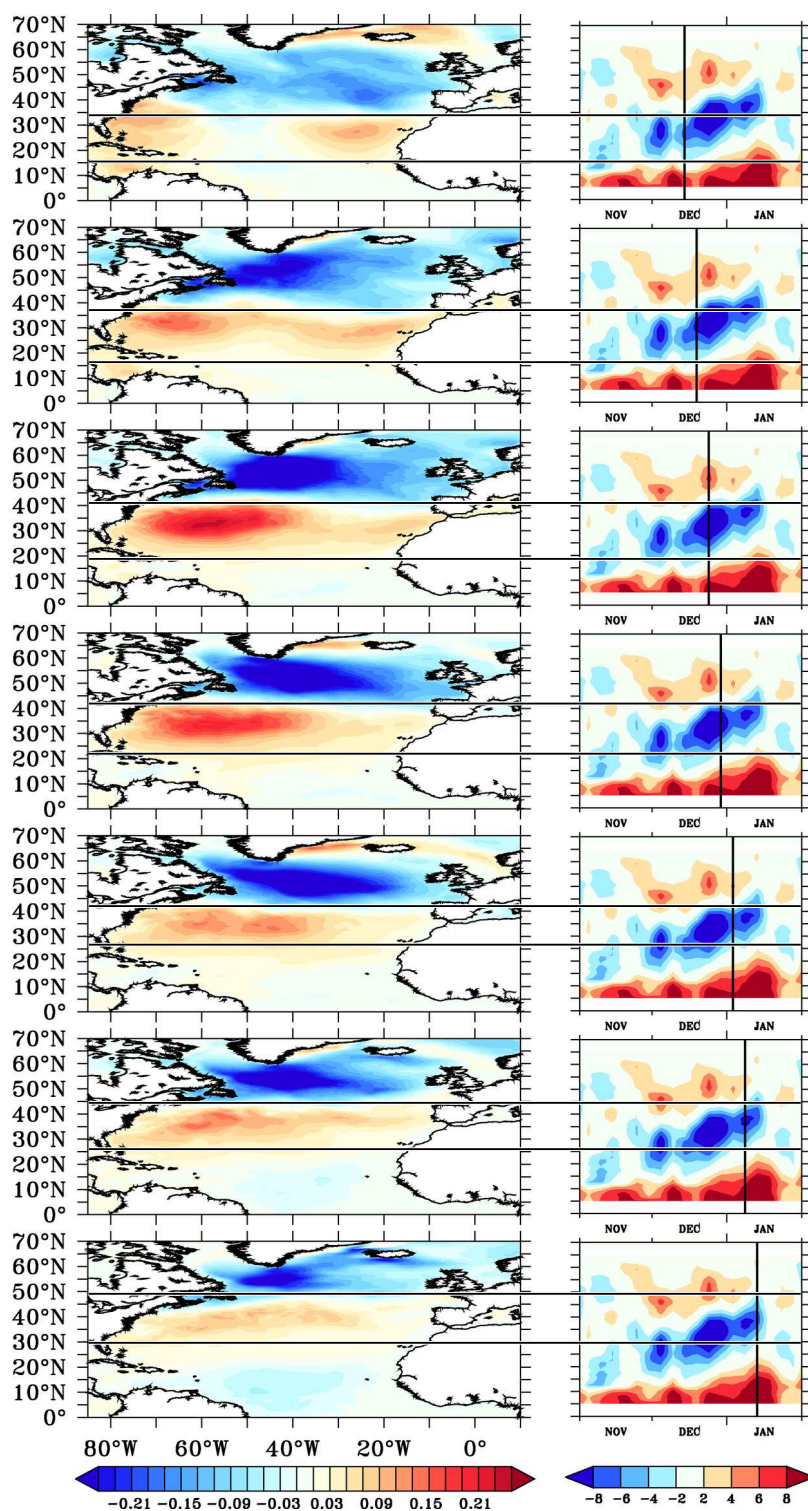


Fig. 5 Sequence of images showing the spatial pattern of zonal wind stress anomalies (Nm^{-2}) over the N. Atlantic (left) at the time indicated by the vertical thick black line on the Hovmöller diagram (right). The Hovmöller diagram depicts the anomalous Ekman transport for the winter of 2010/11 (Figure 3b). Horizontal black lines intersect the vertical thick black line at the -2 Sv contour interval, and extend across the panels on the left to indicate the meridional extent of the wind stress anomaly. The data plotted here are 5 day mean values from simulation VN206, smoothed using a 15 day Parzen filter.

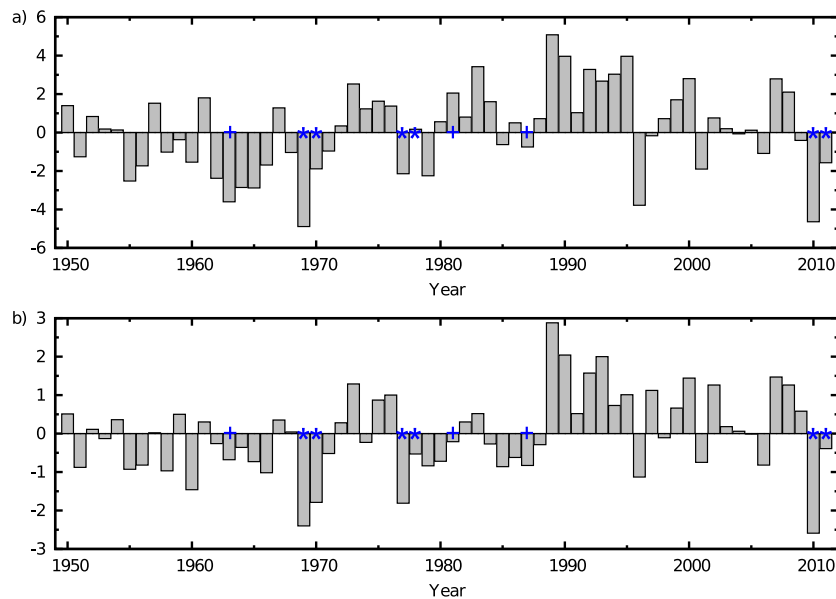


Fig. 6 Time series of a) the winter (DJFM) NAO index, and b) the winter (DJFM) AO index (Hurrell (1995); NCAR (2012a)). The events discussed in the text are indicated with * (pair events) and + (single events).

277 3.4 Atmospheric and SST conditions

278 One of the most prominent atmospheric features in the North Atlantic sector is the North
 279 Atlantic Oscillation (NAO). The NAO is an important mode of climate variability which
 280 influences the climate over the North Atlantic and much of northern Europe, particularly
 281 during the winter months. The NAO can be represented by an index, and the one we use
 282 is computed from winter (DJFM) differences between the normalised sea level pressure
 283 (SLP) measured at Lisbon, Portugal and Stykkisholmur, Iceland (Figure 6a, Hurrell (1995);
 284 NCAR (2012a)). When the NAO index is negative the corresponding sea level pressure
 285 anomalies (low over Azores, high over Iceland) drive a southward excursion of the core
 286 of the jet stream, which brings with it cold European winters (Luo et al, 2010). The low
 287 frequency mode of variability which appears in the AMOC anomalies (Figure 3) is positively
 288 correlated (0.65) with the winter NAO variability (Figure 6a). The winter mean NAO index
 289 is predominantly negative between 1950 and 1980 and then transitions to being predominantly
 290 positive from 1980 to 2000. The ocean is thought to influence the low frequency component
 291 of the NAO (Bellucci et al, 2008; Marshall et al, 2000; D'Andrea et al, 2005; Gastineau et al,
 292 2013; Ciasto et al, 2011; Sevellec and Fedorov, 2013). A recent study by Sonnewald et al
 293 (2013) indicates that upper ocean heat content variability in the North Atlantic is dominated
 294 by the ocean heat transport on longer than seasonal timescales. This is supported by an
 295 observation based study which examines the ocean heat content, SST and surface fluxes
 296 associated with the events of 2009-2011, and finds that reduction in the strength of the
 297 AMOC was primarily responsible for the observed anomalous heat content (Bryden et al,
 298 2014). Potential predictability of the AMOC can account for forecast skill of North Atlantic
 299 SST, particularly for the subpolar gyre (see Hermanson et al (2014) and references therein).

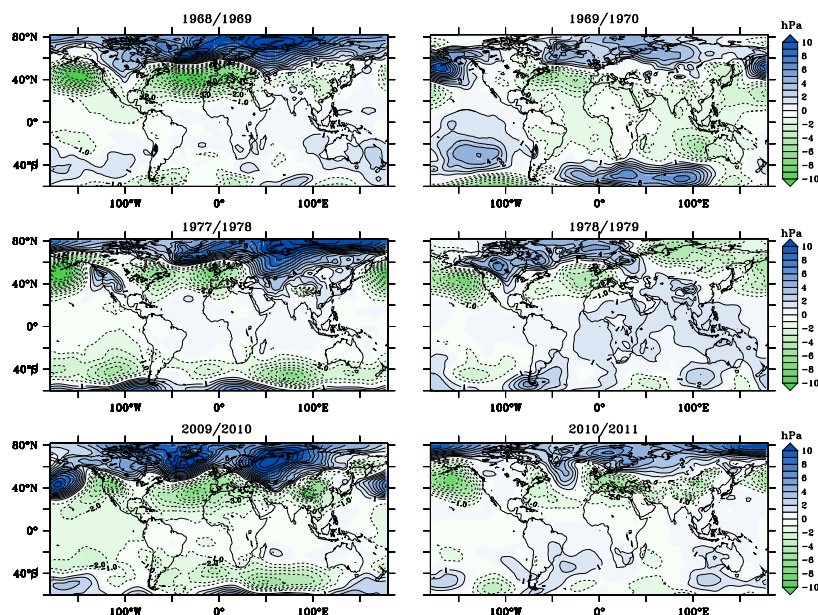


Fig. 7 Winter mean sea level pressure anomalies calculated from the NCEP/NCAR reanalysis dataset for years in which a pair of AMOC minima are seen in consecutive winters. Events shown are 1969/70 (top), 1978/79 (middle), and 2010/11 (bottom). The winter of the first year is shown on the left and for the following year on the right.

300 Together, this increasing body of literature supports the idea that the ocean is an important
 301 contributor to low frequency atmospheric variability.

302 Examining first the most recent events, the winters of 2009/10 and 2010/11 both exhib-
 303 ited a strongly negative NAO index, with December 2010 recording the second lowest NAO
 304 index (-4.62) since records began in 1825 (Osborn, 2011). Spatial plots of the winter mean
 305 SLP for the winters of 2009/10 and 2010/11 (Figure 7e,f) show that these winters, that of
 306 2009/10 in particular, bear the characteristics of a negative Arctic oscillation (AO) pattern
 307 with a pronounced anomaly in the N. Atlantic sector and over Russia. The AO is another
 308 pattern of atmospheric variability closely related to the NAO (Figure 6b), and is derived us-
 309 ing the first principle component of winter (DJFM) sea level pressure anomalies poleward of
 310 20°N (NCAR, 2012b). However, whilst the two indices are closely related, strongly negative
 311 AO years do not necessarily coincide with a strongly negative NAO. The NAO is considered
 312 by some to be a regional expression of the AO (see e.g. Thompson and Wallace (2000)),
 313 and Wallace (2000) suggested that they can be considered manifestations of the same basic
 314 phenomenon. February 2010 recorded the lowest AO index (-4.266) since reliable records
 315 began in 1950 (L'Heureux et al, 2010; NOAA, 2013). Similar spatial plots for the winters of
 316 the other pairs of events in 1968/69 - 1969/70 and 1977/78 - 1978/79 reveal that the winters
 317 of the first year of the pair all exhibit similar strong negative AO conditions. The anomaly
 318 patterns, particularly over the North Atlantic sector, are seen in each case to persist in the
 319 following winter.

320 In comparison if we examine the winter mean SLP for three winters in which strong
 321 individual AMOC anomaly events occur (1962/63, 1980/81, 1987/88) the anomaly pattern
 322 is not consistent (Figure 8). For the winter of 1962/63 a strong negative NAO event oc-

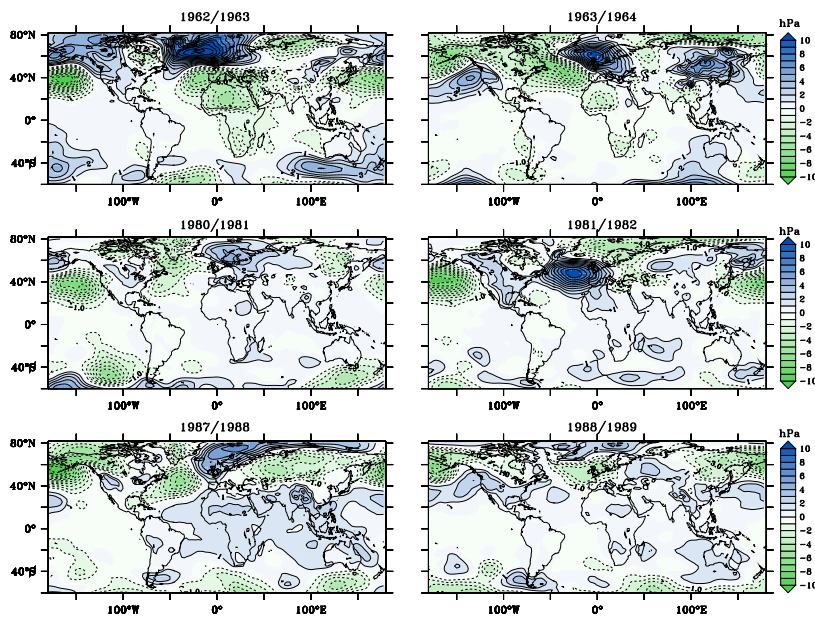


Fig. 8 Winter mean sea level pressure anomalies calculated from the NCEP/NCAR reanalysis dataset for years in which a single minima is seen. Events shown are the winters of 1962/63 (top), 1980/81 (middle), and 1986/87 (bottom). The winter of this year is shown on the left and for the following year when no AMOC minima is seen on the right.

323 curs, but for the winters of 1980/81 and 1987/88 the anomalies indicate a negative Atlantic
 324 ridge (AR) weather pattern. The subsequent winters do not retain the same SLP anomaly
 325 pattern over the N. Atlantic sector. The winter of 1963/64 exhibits a negative AR pattern,
 326 whilst 1981/82 shows a similarly strong positive occurrence of the AR pattern. The winter of
 327 1988/89 exhibits a weak negative NAO pattern.

328 Examining surface air temperature (SAT) anomalies for 1968/69 - 1969/70, 1977/78 -
 329 1978/79 and 2009/10 - 2010/11 reveals a widespread cool anomaly across much of Siberia
 330 for the winters of the pairs of events (Figure 9). For the years associated with single events
 331 cool anomalies are weaker and located over Europe (Figure 10). The temperature anomalies
 332 associated with the pairs of events also show the tendency to persist for the following winter.
 333 This is most pronounced for the winters of 2009/10 and 2010/11 where the cold anomalies
 334 over Eurasia and North America occur mainly over the same regions. For the other two
 335 pairs of events the largest anomalies in the 2m air temperature vary in location from one
 336 year to the next. For the 1968/69 - 1969/70 pair the first event coincided with exception-
 337 ally low temperatures over Siberia (e.g. Hirschi and Sinha (2007)), whilst anomalies were
 338 small over Europe. During the second event in contrast the coldest anomalies occurred over
 339 Northwestern Europe. A large variability in the temperature distribution in different NAO
 340 negative winters is consistent with earlier studies (e.g. Heape et al (2013)).

341 Taws et al (2011) present evidence that SST anomaly patterns in the North Atlantic dur-
 342 ing the winter of 2010/11 arose from the re-emergence of a remnant tripole pattern of SST
 343 anomalies formed during the winter of 2009/2010 (Figure 11). The anomaly pattern is char-
 344 acterised by a tripole of warm anomalies in and around the Labrador Sea, cold anomalies
 345 which extend across much of the North Atlantic from around 25°N to 50°N, and a warm

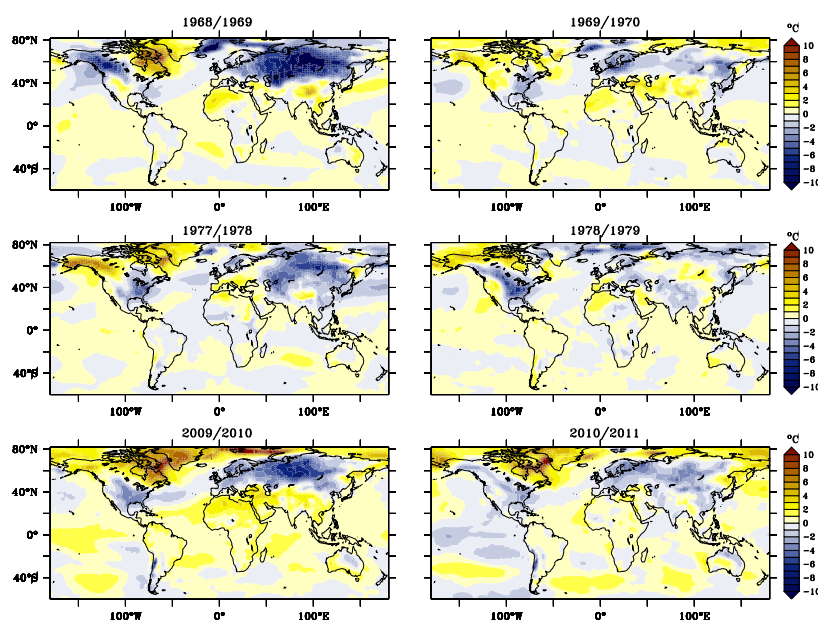


Fig. 9 Winter mean surface air temperature anomalies calculated from the NCEP/NCAR reanalysis dataset for years in which a pair of AMOC minima are seen in consecutive winters. Events shown are 1969/70 (top), 1978/79 (middle), and 2010/11 (bottom). The winter of the first year is shown on the left and for the following year on the right.

346 anomaly south of 25°N . The SST anomalies for January and February of 2010 (not shown)
 347 are similar in amplitude and spatial pattern to March. Re-emergence of temperature anom-
 348 alies provides a mechanism by which anomalous SST conditions can persist from one winter
 349 to the next (Alexander and Deser, 1995). A recent paper by Buchan et al (2014) examines the
 350 response of a coupled climate model to the inclusion of SST anomalies observed during the
 351 years of 2009 and 2010. The inclusion of the anomalies is shown to result in a statistically
 352 significant negative shift of the NAO in the model, supporting the idea that re-emergence
 353 of an SST anomaly pattern may influence the atmosphere and contribute to the necessary
 354 conditions for persistence of negative NAO conditions and extreme cold winter weather over
 355 northwest Europe. An earlier study by Cassou et al (2007) also found the SST anomaly pat-
 356 tern associated with re-emergence led to an atmospheric circulation which resembled the
 357 one from the previous winter.

358 The atmospheric conditions during the winters of 1968/69 and 1977/78 were similar to
 359 those experienced in the winter of 2009/10, with the NAO and AO indices in an extreme
 360 negative state (Figure 6). Taws (2013) examined SST fields from EN3 for evidence of pre-
 361 vious re-emergence signatures. Figure 12a shows lagged pattern correlations referenced to
 362 March (March through to April of the following year) of SST anomalies for the North At-
 363 lantic computed from EN3 (Ingleby and Huddleston, 2007). It shows that both March 2010
 364 and the following winter and March 1969 and the following winter exhibited higher lev-
 365 els of correlation (between 1 and 2 standard deviations of the 1950-2011 period) between
 366 subsequent winters, and the similarity of the timing and strength of the correlation suggests
 367 that both periods experienced re-emergence events. March of 1978 and the following winter
 368 show no significant increased correlation, suggesting that re-emergence did not occur during

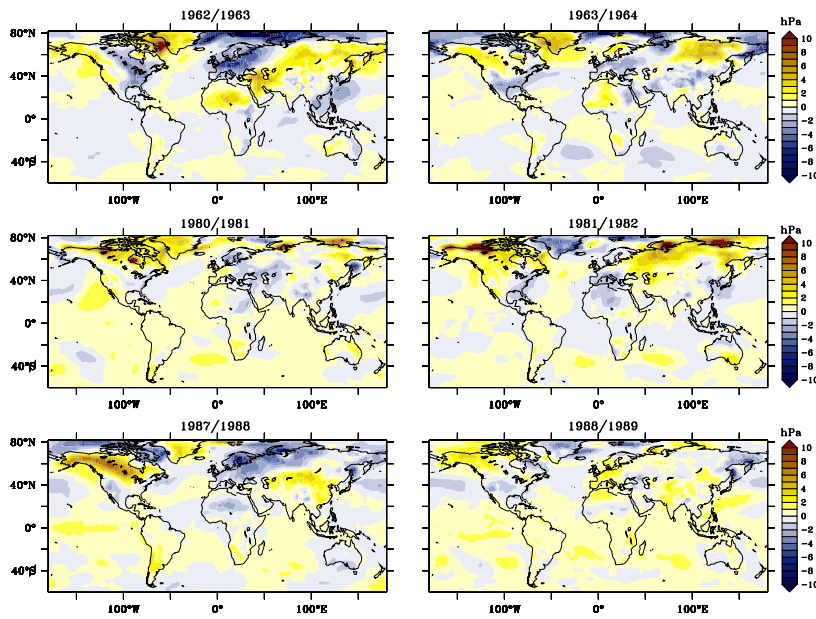


Fig. 10 Winter mean surface air temperature anomalies calculated from the NCEP/NCAR reanalysis dataset for years in which a single minima is seen. Events shown are the winters of 1962/63 (top), 1980/81 (middle), and 1986/87 (bottom). The winter of this year is shown on the left and for the following year when no AMOC minima is seen on the right.

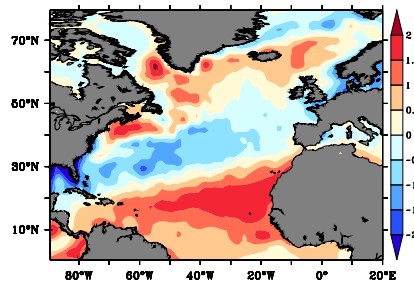


Fig. 11 March 2010 SST anomalies obtained from the NOAA OI dataset.

369 this period. None of the other years show a strong indication of re-emergence. Figure 12b is
 370 equivalent to 12a, but instead shows a composite of the lagged pattern correlations computed
 371 from SST anomalies in the ensemble of ORCA025 models. The models also show signifi-
 372 cantly higher correlations between the winter months of 1968 and 1969, in this case between
 373 2 and 3 standard deviations, indicating that there was a re-emergence event. The model en-
 374 semble also found no significant correlation between March 1978 and the following winter,
 375 indicating that this period did not experience a re-emergence event.

376 To further examine the strong indicators of reemergence for 1968/69 we plot surface
 377 and subsurface temperature anomalies for the region 5-65°N, 80-10°W. An SST anomaly
 378 pattern similar in amplitude and distribution to the one presented in Figure 11) is present
 379 in March 1969 (Figure 13 a). After persistent AO negative atmospheric conditions over

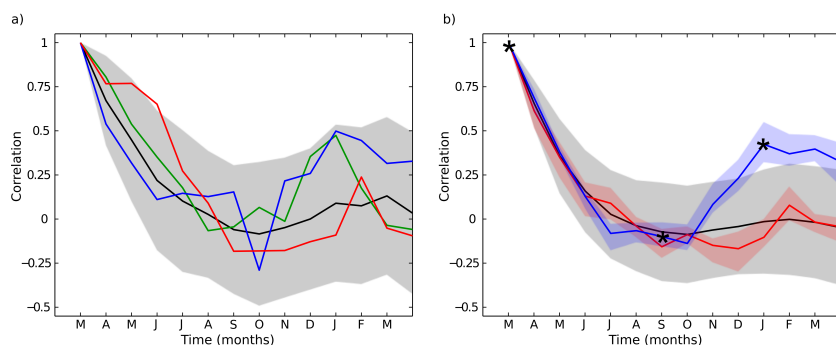


Fig. 12 One-year pattern correlation function for North Atlantic SSTAs ($5\text{-}65^\circ\text{N}$, $80\text{-}10^\circ\text{W}$). a) shows correlations from EN3 from March 2010-March 2011 (green), March 1969-March 1970 (blue), March 1978-March 1979 (red), and a 50-year (1960-2011) average (black). b) shows the equivalent from the five simulations which comprise the NEMO ORCA025 ensemble. March 1969-March 1970 (blue) and March 1978-March 1979 (red) are shown. The lighter overlay for each line shows the range of the ensemble. The asterisks on the blue curve indicate the dates in 1969/70 which are presented in Figure 13. For both panels the grey shading denotes the range (2 standard deviations) of correlation found in the a) 1950-2011 and b) 1958-2001 periods.

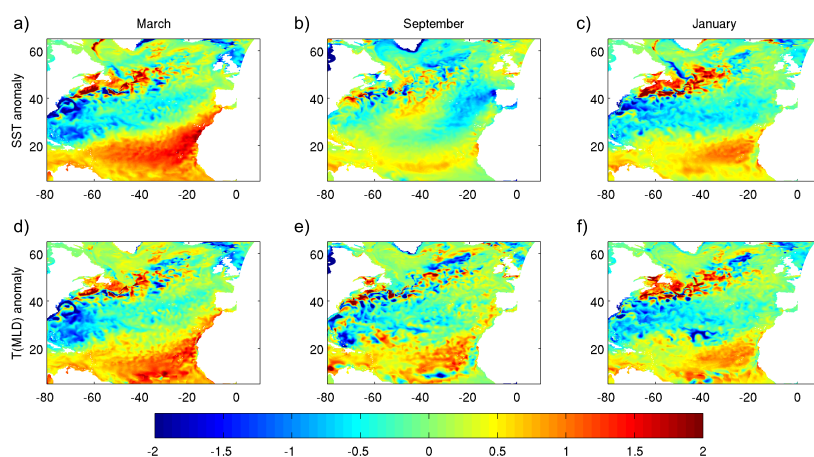


Fig. 13 Evolution of temperature anomalies from March 1969 to January 1970. SST anomalies (top row) and temperature anomalies at the base of the winter mixed layer (bottom row) from simulation N102 are shown for March 1969 (left column), September 1969 (middle column) and January 1970 (right column). Data are low pass filtered and then a mean seasonal cycle is removed.

380 the winter months this anomaly is coherent down to the base of the winter mixed layer
 381 (Figure 13 d). The pattern continues to persist into September at the winter mean mixed
 382 layer depth, below the shallow summer mixed layer (Figure 13 e), and through to January of
 383 1970 (Figure 13f), where the seasonal mixing returns the anomaly to the surface (Figure 13
 384 c). The SST anomaly in September of 1969 (Figure 13 b) is uncorrelated with the SST
 385 anomaly present in March 1969 (see Figure 12b).

386 The mechanism of re-emergence, whereby temperature anomalies formed in the deep
 387 winter mixed layer are trapped subsurface by the shallow summer mixed layer and then
 388 re-entrained into the mixed layer during the onset of the following winter occurs annu-
 389 ally. However, in order to provide a memory to the atmosphere a strong and coherent SST

390 anomaly pattern must form during the first winter. A strong negative AO or NAO state
391 which is persistent throughout the winter would facilitate this. There are a number of in-
392 dividual AMOC minima events which occur in the composite time series (Figure 2), some
393 of which are associated with negative NAO states, some of which are not. A possible ex-
394 planation for why re-emergence events only occurred during strong negative AO states is
395 that these events are consistently stable over the North Atlantic sector throughout winter
396 (December to March). To examine this we construct a time series of the maximum monthly
397 NAO index occurring during the winter months (DJFM). The mean and standard deviation
398 of this time series are 1.7 and 1.22 respectively. For the 1968/69 and 2009/10 winters the
399 maximum monthly mean NAO index reached during winter was -1.4 and -1.5 respectively,
400 around 2.5 standard deviations lower than the mean winter maximum. The maximum NAO
401 index during winter of 1977/78 was also anomalously low at -0.5, 1.75 standard deviations
402 below the mean. The winter maximum NAO index for the three individual events examined
403 (1962/63, 1980/81 and 1987/88) were all within 0.5 standard deviations of the mean.

404 Interestingly the responses in the AMOC are stronger for 1978/79 than for 1969/70,
405 indicating that processes other than re-emergence might be important for providing memory
406 to the atmosphere from one winter to the next, resulting in the wind stress anomalies which
407 provide the Ekman anomaly in two consecutive winters. Of course it is also possible that
408 two consecutive events occur by chance, and that no processes for providing memory from
409 one winter to the next are involved.

410 **4 Summary and discussion**

411 In light of the anomalous minima events recorded in the AMOC for the winters of 2009/10
412 and 2010/11 by the 26°N array (McCarthy et al, 2012) we employ an ensemble comprising
413 five 1/4° ocean model realisations to investigate how frequently these events have occurred
414 in the past, and in particular whether there are mechanisms which might give rise to multiple
415 events occurring in consecutive winters.

416 We first make comparisons between two model integrations (one 1/4° and one 1/12°)
417 which cover the period for which we have observations and determine that the NEMO
418 ORCA ocean model is able to adequately reproduce the interannual variability of the AMOC
419 captured by the mooring array, as well as the timing and amplitude of the anomalously strong
420 minima which occur during the winter's of 2009/10 and 2010/11. The model is not able to
421 capture all of the variability seen in the observations, and we do not expect it to given that
422 around 30% of the variability is chaotic (Hirschi et al, 2013). The modelled amplitudes of
423 the 2009/10 and 2010/11 events are slightly lower than observed, but so are both the mean
424 and standard deviation of the AMOC represented in the model.

425 Examining the ensemble of NEMO runs which extend back to 1958 we have identified
426 a number of events for which a strong reduction of the AMOC transport occurred. In some
427 cases (e.g. 1962) these are individual events, but we also identify two pairs of events which
428 occur in consecutive years during 1969/70 and 1978/79, which are historical analogues of
429 the recently observed events. A possible third weaker analogue occurred in 1997/98.

430 We compare boreal winter atmospheric conditions for the years during which extreme
431 negative anomalies in the AMOC were observed. The AMOC minimum event which oc-
432 curred in the winter of 1962 coincides with an extended period of negative NAO, but no
433 significant AO index. Other examples of individual events such as in 1981 and 1990 do not
434 coincide with negative NAO states. In fact 1990 corresponds to one of the strongest positive
435 AO and NAO indices for the period we examine. The pairs of events identified in 1969/70,

436 1978/79 and 2010/11 are all associated with strong negative AO indices, with particularly
437 strong SLP patterns over the North Atlantic sector, and corresponding with strongly negative
438 NAO indices. The event in the winter of 2009/10 coincides with one of the strongest nega-
439 tive values of the NAO index since records began in 1860, and there is evidence that the re-
440 emergence mechanism contributed to persistence of the SST anomalies (Taws et al, 2011),
441 and to the renewed development of negative NAO conditions (Buchan et al, 2014). We show
442 here that the events of 1968/69 are also connected to an occurrence of re-emergence, but
443 the equally strong, if not stronger, AMOC minima seen in 1978/79 are not linked to a re-
444 emergence of SST anomalies. Surface air temperature anomalies for all 3 events in 1969/70,
445 1978/79 and 2010/11 show a strong negative anomaly which covers much of Siberia, and
446 other studies suggest that mechanisms related to sea ice cover over the Arctic and North
447 Atlantic (e.g. Deser et al (2007)) or to snow cover and thickness over Eurasia (Peings et al,
448 2012; Fletcher et al, 2009; Gong et al, 2004, 2003) may provide memory to the atmosphere
449 which allows the negative NAO conditions over the North Atlantic sector to persist.

450 The minimum of the events frequently coincides with anomalously strong southward
451 Ekman transport, which constitutes around half of the anomaly. We find that the simulations
452 also capture a substantial amount of the low frequency variability of the UMO transport,
453 indicating that this signal is also surface forced. It may be Sverdrup transport (Duchez et al,
454 2014b) or relates to other mechanisms such as a lagged ocean response to the surface forcing
455 such as the one described by Sinha et al (2013), whereby changes in windstress influence
456 ocean transport through adjustments of the vertical velocity and vortex stretching. Some of
457 the model runs respond strongly for a given event whilst others show weaker responses,
458 indicating that the events are not purely a response to the surface forcing but that there is
459 some dependence on the ocean state or that ocean physics may affect the strength or timing
460 of the non-Ekman component of the anomalies. For example, a study which compared two
461 of the simulations used here (N102 and N112) found that up to 30% of the total variability
462 of the AMOC is attributable to chaotic processes such as mesoscale eddies and internal and
463 planetary waves (Hirschi et al, 2013). Bryden et al (2014) examine the 2009/10 event and
464 conclude that some of the observed reduction is due to modes of ocean variability which are
465 not associated with recent atmospheric forcing. Understanding these modes of variability
466 could lead to improvements in the model representation of such events.

467 An interesting implication of the association of the extreme negative events with nega-
468 tive AO patterns and the re-emergence of SST anomalies is that it may be possible to predict
469 the onset of negative NAO conditions and a second consecutive AMOC minimum (Maidens
470 et al, 2013). There may also be scope for improved prediction of the AMOC for a third
471 consecutive winter, since the anomaly composite reveals that there are no cases since 1958
472 where we find three or more consecutive extreme negative events.

473 **Acknowledgements** This work was supported by the RAPID-WATCH project VALOR (NE/G007772/1)
474 and was also part of the DRACKAR project. Data from the RAPID-WATCH MOC monitoring project are
475 funded by the Natural Environment Research Council and are freely available from www.noc.soton.ac.uk/rapidmoc. Sarah Taws was funded by a NERC Quota Studentship, with added support from the UK Met
476 Office. NCEP Reanalysis Derived data were provided by the NOAA/OAR/ESRL PSD, Boulder, Colorado,
477 USA, from their Web site at <http://www.esrl.noaa.gov/psd/>. NAO Index Data was provided by the
478 Climate Analysis Section, NCAR, Boulder, USA. We thank two anonymous reviewers for their useful and
479 constructive comments.
480

481 **References**

- 482 Alexander MA, Deser C (1995) A mechanism for the recurrence of wintertime mid-latitude
483 SST anomalies. *Journal of Physical Oceanography* 25:122–137
- 484 Baehr J, Haak H, Alderson S, Cunningham SA, Jungclaus JH, Marotzke J (2007) Timely
485 detection of changes in the meridional overturning circulation at 26N in the Atlantic.
486 *Journal of Climate* 20(23):5827–5841
- 487 Baehr J, Cunningham SA, Haak H, Heimbach P, Kanzow T, Marotzke J (2009) Observed
488 and simulated daily variability of the meridional overturning circulation at 26.5°N in the
489 Atlantic. *Ocean Science Discussions* 5:575–589
- 490 Balan Sarojini B, Gregory J, Tailleux R, Bigg GR, Blaker AT, Cameron DR, Edwards NR,
491 Megann AP, Shaffrey L, Sinha B (2011) High frequency variability of the Atlantic merid-
492 ional overturning circulation. *Ocean Science* 7(4):471–486, doi:10.5194/os-7-471-2011
- 493 Barnier B, Madec G, Penduff T, Molines JM, Treguier AM, Sommer JL, Beckmann A, Bias-
494 toch A, Bning C, Dengg J, Derval C, Durand E, Gulev S, Remy E, Talandier C, Theetten
495 S, Maltrud M, McClean J, de Cuevas B (2006) Impact of partial steps and momentum ad-
496 vection schemes in a global ocean circulation model at eddy-permitting resolution. *Ocean*
497 *Dynamics* 56:543–567
- 498 Bellucci A, Gualdi S, Scoccimarro E, Navarra A (2008) NAO–ocean circulation interactions
499 in a coupled general circulation model. *Climate Dynamics* 31(7–8):759–777
- 500 Blaker AT, Hirschi JJM, Sinha B, de Cuevas BA, Alderson SG, Coward AC, Madec G (2012)
501 Large near-inertial oscillations of the Atlantic meridional overturning circulation. *Ocean*
502 *Modelling* 42:50–56, doi:10.1016/j.ocemod.2011.11.008
- 503 Brodeau L, Barnier B, Penduff T, Treguier AM, Gulev S (2010) An ERA 40 based atmo-
504 spheric forcing for global ocean circulation models. *Ocean Modelling* 31(3–4):88–104
- 505 Broecker WS (1987) The biggest chill. *Natural History Magazine* 97:74–82
- 506 Bryden H, King BA, McCarthy GD, McDonagh EL (2014) Impact of a 30% reduction in
507 Atlantic meridional overturning during 2009–2010. *Ocean Science Discussions* 11:789–
508 810
- 509 Buchan J, Hirschi JJM, Blaker AT, Sinha B (2014) Influence of North Atlantic Sea Sur-
510 face Temperature anomalies on the NAO in December 2010. *Monthly Weather Review*
511 142:922–932
- 512 Cassou C, Deser C, Alexander MA (2007) Investigating the Impact of Reemerging Sea
513 Surface Temperature Anomalies on the Winter Atmospheric Circulation over the North
514 Atlantic. *Journal of Climate* 20:3510–3526, doi:10.1175/JCLI4202.1
- 515 Chidichimo MP, Kanzow T, Cunningham SA, Johns WE, Marotzke J (2010) The contribu-
516 tion of eastern-boundary density variations to the Atlantic meridional overturning cir-
517 culation at 26.5N. *Ocean Science* 6:475–490
- 518 Ciasto LM, Alexander MA, Deser C, England MH (2011) On the Persistence of Cold-
519 Season SST Anomalies Associated with the Annular Modes. *Journal of Climate*
520 24(10):2500–2515
- 521 Cunningham SA, Kanzow T, Rayner D, Baringer MO, Johns WE, Marotzke J, Longworth
522 HR, Grant EM, Hirschi JJM, Beal LM, Meinen CS, Bryden HL (2007) Temporal vari-
523 ability of the Atlantic meridional overturning circulation at 26.5n. *Science* 317(5840)
- 524 D’Andrea F, Czaja A, Marshall J (2005) Impact of Anomalous Ocean Heat Transport on the
525 North Atlantic Oscillation. *Journal of Climate* 18(23):4955–4969
- 526 Dee DP, Uppala SM, Simmons AJ, Berrisford P, Poli P, Kobayashi S, Andrae U, Balmaseda
527 MA, Balsamo G, Bauer P, Bechtold P, Beljaars ACM, van de Berg L, Bidlot J, Bor-
528 mann N, Delsol C, Dragani R, Fuentes M, Geer AJ, Haimberger L, Healy SB, Hersbach

- 529 H, Hlm EV, Isaksen L, Killberg P, Khler M, Matricardi M, McNally AP, Monge-Sanz
530 BM, Morcrette JJ, Park BK, Peubey C, de Rosnay P, Tavalato C, Thpaut JN, Vitart F
531 (2011) The ERA-Interim reanalysis: configuration and performance of the data assimila-
532 tion system. *Quarterly Journal of the Royal Meteorological Society* 137(656):553–597,
533 doi: 10.1002/qj.828
- 534 Deser C, Tomas RA, Peng S (2007) The Transient Atmospheric Circulation Response to
535 North Atlantic SST and Sea Ice Anomalies. *Journal of Climate* 20(18):4751–4767
- 536 Deshayes J, Treguier AM, Barnier B, Lecointre A, Sommer JL, Molines JM, Penduff T,
537 Bourdalle-Badie R, Drillet Y, Garric G, Benshilla R, Madec G, Biastoch A, Boning
538 CW, Scheinert M, Coward AC, Hirschi JJM (2013) Oceanic hindcast simulations at
539 high resolution suggest that the Atlantic MOC is bistable. *Geophysical Research Letters*
540 40(12):3069–3073, doi:10.1002/grl.50534
- 541 Dickson RR, Brown J (1994) The production of North Atlantic Deep Water: Sources,
542 rates, and pathways. *Journal of Geophysical Research - Oceans* 99(C6):12,319–12,341,
543 doi:10.1029/94JC00530
- 544 DRAKKAR Group (2007) Eddy-permitting ocean circulation hindcasts of past decades.
545 *CLIVAR Exchanges* 12(3):8–10
- 546 Duchez A, Frajka-Williams E, Castro N, Hirschi JJM, Coward A (2014a) Seasonal to inter-
547 annual variability in density around the Canary Islands and their influence on the Atlantic
548 meridional overturning circulation at 26N. *Journal of Geophysical Research: Oceans* 119,
549 doi:10.1002/2013JC009416
- 550 Duchez A, Hirschi JJM, Cunningham SA, Blaker AT, Bryden HL, de Cuevas BA, Atkinson
551 CP, McCarthy GD, Frajka-Williams E, Rayner D, Smeed D, Mizielinski MS (2014b) A
552 new index for the Atlantic Meridional Overturning Circulation at 26N. *Journal of Climate*
553 In press
- 554 Fletcher CG, Hardiman SC, Kushnir PJ (2009) The Dynamical Response to Snow Cover
555 Perturbations in a Large Ensemble of Atmospheric GCM Integrations. *Journal of Climate*
556 22:1208–1222
- 557 Ganachaud A, Wunsch C (2000) Improved estimates of global ocean circulation, heat trans-
558 port and mixing from hydrographic data. *Nature* 408:453–457, doi:10.1038/35044048
- 559 Gastineau G, D'Andrea F, Frankignoul C (2013) Atmospheric response to the North Atlantic
560 Ocean variability on seasonal to decadal time scales. *Climate Dynamics* 40(9–10):2311–
561 2330, doi:10.1007/s00382-012-1333-0
- 562 Gong G, Entekhabi D, Cohen J (2003) Modeled Northern Hemisphere Winter Climate
563 Response to Realistic Siberian Snow Anomalies. *Journal of Climate* 16:3917–3931,
564 doi:10.1175/1520-0442(2003)016<3917:MNHWCRCR>2.0.CO;2
- 565 Gong G, Entekhabi D, Cohen J, Robinson D (2004) Sensitivity of atmospheric response to
566 modeled snow anomaly characteristics. *Journal of Geophysical Research* 109(D06107),
567 doi:10.1029/2003JD004160
- 568 Grist JP, Josey SA, Marsh R, Good SA, Coward AC, de Cuevas BA, Alderson SG, New
569 AL, Madec G (2010) The roles of surface heat flux and ocean heat transport convergence
570 in determining Atlantic Ocean temperature variability. *Ocean Dynamics* 60(4):771–790,
571 doi:10.1007/s10236-010-0292-4
- 572 Grist JP, Josey SA, Marsh R (2012) Surface estimates of the Atlantic overturning in density
573 space in an eddy-permitting ocean model. *Journal of Geophysical Research* 117(C06012),
574 doi:10.1029/2011JC007752
- 575 Heape R, Hirschi JJM, Sinha B (2013) Asymmetric response of European pressure and
576 temperature anomalies to NAO positive and NAO negative winters. *Weather* 68(3):73–
577 80, doi:10.1002/wea.2068

- 578 Hermanson L, Eade R, Robinson NH, Dunstone NJ, Andrews MB, Knight JR, Scaife AA,
579 Smith DM (2014) Forecast cooling of the Atlantic subpolar gyre and associated impacts.
580 Geophysical Research Letters doi:10.1002/2014GL060420
- 581 Hirschi J, Marotzke J (2007) Reconstructing the Meridional Overturning Circulation from
582 Boundary Densities and the Zonal Wind Stress. *Journal of Physical Oceanography*
583 37:743–763
- 584 Hirschi J, Baehr J, Marotzke J, Stark J, Cunningham S, Beismann JO (2003) A monitoring
585 design for the Atlantic meridional overturning circulation. *Geophysical Research Letters*
586 30(7):1413, doi:10.1029/2002GL016776
- 587 Hirschi J, Blaker A, Sinha B, de Cuevas B, Alderson SG, Coward AC, Madec G (2013)
588 Chaotic variability of the meridional overturning circulation on subannual to interannual
589 timescales. *Ocean Science* 9:3191–3238, doi:10.5194/osd-9-3191-2012
- 590 Hirschi JJM, Sinha B (2007) Negative NAO and cold Eurasian winters: how exceptional
591 was the winter of 1962/1963? *Weather* 62(2):43–48, doi:10.1002/wea.34
- 592 Hurrell JW (1995) Decadal trends in the North Atlantic Oscillation regional temperatures
593 and precipitation. *Science* 269:676–679
- 594 Ingleby B, Huddleston M (2007) Quality control of ocean temperature and salinity
595 profiles - historical and real-time data. *Journal of Marine Systems* 65:158–175,
596 doi:10.1016/j.jmarsys.2005.11.019
- 597 Johns WE, Baringer MO, Beal LM, Cunningham SA, Kanzow T, Bryden HL, Hirschi JJM,
598 Marotzke J, Meinen C, Shaw B, Curry R (2011) Continuous, array-based estimates of
599 Atlantic Ocean heat transport at 26.5N. *Journal of Climate* 0(0):00–00
- 600 Jourdan D, Balopoulos E, Garcia-Fernandez M, Maillard C (1998) Objective analysis of
601 temperature and salinity historical data set over the mediterranean basin. Technical report
602 IEEE
- 603 Kalnay E, Kanamitsu M, Kistler R, Collins W, Deaven D, Gandin L, Iredell M, Saha S,
604 White G, Woollen J, Zhu Y, Chelliah M, Ebisuzaki W, Higgins W, Janowiak J, Mo
605 KC, Ropelewski C, Wang J, Leetmaa A, Reynolds R, Jenne R, Joseph D (1996) The
606 NCEP/NCAR 40-year reanalysis project. *Bull Am Meteorol Soc* 77:437–471
- 607 Kanzow T, Johnson HL, Marshall DP, Cunningham SA, Hirschi JJM, Mujahid A, Bryden
608 HL, Johns WE (2009) Basinwide integrated volume transports in an eddy-filled ocean.
609 *Journal of Physical Oceanography* 39:3091–3110, doi: 10.1175/2009JPO4185.1
- 610 Kanzow T, Cunningham SA, Johns WE, Hirschi JJM, Baringer MO, Meinen CS,
611 Chidichimo MP, Atkinson CP, Beal LM, Bryden HL, Collins J (2010) Seasonal vari-
612 ability of the Atlantic meridional overturning circulation at 26.5N. *Journal of Climate*
613 23:5678–5698
- 614 Kuhlbrodt T, Griesel A, Montoya M, Levermann A, Hofmann M, Rahmstorf S (2007) On
615 the driving processes of the Atlantic meridional overturning circulation. *Reviews in Geo-*
616 *physics* 45(RG2001), doi:10.1029/2004RG000166
- 617 Large WG, Yeager SG (2004) Diurnal to decadal global forcing for ocean and sea-ice mod-
618 els: The data sets and flux climatologies. Technical Report TN-460+STR(NCAR):105pp
- 619 Large WG, Yeager SG (2008) The Global Climatology of an Interannually Varying Air-Sea
620 Flux Data Set. *Climate Dynamics* Doi:10.1007/s00382-008-0441-3
- 621 Levitus S, Conkright M, Boyer TP, O’Brian T, Antonov J, Stephens C, Johnson LSD, Gelfeld
622 R (1998) World Ocean Database 1998. Technical report NESDIS 18, NOAA Atlas:346pp
- 623 L’Heureux M, Butler A, Jha B, Kumar A, Wang W (2010) Unusual extremes in the negative
624 phase of the Arctic Oscillation during 2009. *Geophysical Research Letters* 37(L10704),
625 doi:10.1029/2010GL043338

- 626 Lumpkin R, Speer K (2007) Global Ocean Meridional Overturning. *Journal of Physical*
627 *Oceanography* 37:2550–2562
- 628 Luo D, Zhu Z, Ren R, Zhong L, Wang C (2010) Spatial Pattern and Zonal Shift of the North
629 Atlantic Oscillation. Part I: A Dynamical Interpretation. *Journal of Atmospheric Science*
630 67:2805–2826, doi:10.1175/2010JAS3345.1
- 631 Madec G (2008) NEMO ocean engine. Note du Pole de modélisation, Institut Pierre-Simon
632 Laplace (IPSL), France 27:1288–1619
- 633 Maidens A, Arribas A, Scaife AA, Maclachlan C, Peterson D, Knight J (2013) The Influence
634 of Surface Forcings on Prediction of the North Atlantic Oscillation Regime of Winter
635 2010–11. *Monthly Weather Review* XX, in preparation
- 636 Marshall J, Johnson H, Goodman J (2000) A Study of the Interaction of the North Atlantic
637 Oscillation with Ocean Circulation. *Journal of Climate* 14:1399–1421, doi:10.1175/1520-
638 0442(2001)014<1399:ASOTIO>2.0.CO;2
- 639 McCarthy G, Frajka-Williams E, Johns WE, Baringer MO, Meinen CS, Bryden HL, Rayner
640 D, Duchez A, Cunningham SA (2012) Observed Interannual Variability of the Atlantic
641 Meridional Overturning Circulation at 26.5N. *Geophysical Research Letters* 39(L19609),
642 doi:10.1029/2012GL052933
- 643 NCAR (2012a) The Climate Data Guide: Hurrell North Atlantic Oscillation (NAO)
644 Index (station-based). URL [http://climatedataguide.ucar.edu/guidance/
645 hurrell-north-atlantic-oscillation-nao-index-station-based](http://climatedataguide.ucar.edu/guidance/hurrell-north-atlantic-oscillation-nao-index-station-based)
- 646 NCAR (2012b) The Climate Data Guide: Hurrell wintertime SLP-based Northern An-
647 nular Mode (NAM) Index. URL [http://climatedataguide.ucar.edu/guidance/
648 hurrell-wintertime-slp-based-northern-annular-mode-nam-index](http://climatedataguide.ucar.edu/guidance/hurrell-wintertime-slp-based-northern-annular-mode-nam-index)
- 649 NOAA (2013) 2009/2010 Cold Season. URL [http://www.ncdc.noaa.gov/
650 special-reports/2009-2010-cold-season.html](http://www.ncdc.noaa.gov/special-reports/2009-2010-cold-season.html)
- 651 Osborn TJ (2011) Winter 2009/2010 temperatures and a record breaking North Atlantic
652 Oscillation index. *Weather* 66:19–21
- 653 Peings Y, Saint-Martin D, Douville H (2012) A numerical sensitivity study of the influ-
654 ence of siberian snow on the northern annular mode. *Journal of Climate* 25:592–607,
655 doi:10.1175/JCLI-D-11-00038.1
- 656 Quartly GD, de Cuevas BA, Coward AC (2013) Mozambique Channel Eddies in GCMs: A
657 question of resolution and slippage. *Ocean Modelling* 63:56–67
- 658 Rayner D, Hirschi JJM, Kanzow T, Johns WE, Wright PG, Frajka-Williams E, Bryden HL,
659 Meinen CS, Baringer MO, Marotzke J, Beal LM, Cunningham SA (2011) Monitoring the
660 Atlantic meridional overturning circulation. *Deep Sea Research Part II: Topical Studies*
661 *in Oceanography* 58(17–18):1744–1753
- 662 Reynolds RW, Rayner NA, Smith TM, Stokes DC, Wang W (2002) An improved in situ and
663 satellite sst analysis for climate. *Journal of Climate* 15:1609–1625
- 664 Rhines PB, Häkkinen S (2003) Is the Oceanic Heat Transport in the North Atlantic Irrelevant
665 to the Climate in Europe? *ASOF Newsletter* 1:13–17
- 666 Sevellec F, Fedorov AV (2013) The Leading, Interdecadal Eigenmode of the Atlantic Merid-
667 ional Overturning Circulation in a Realistic Ocean Model. *Journal of Climate* 26:2160–
668 2183, doi:10.1175/JCLI-D-11-00023.1
- 669 Sevellec F, Hirschi JJM, Blaker AT (2014) On the super-inertial resonance of the Atlantic
670 meridional overturning circulation. *Journal of Physical Oceanography* 43:2661–2672,
671 doi:10.1175/JPO-D-13-092.1
- 672 Sinha B, Blaker AT, Hirschi JJM, Bonham S, Brand M, Josey S, Smith R, Marotzke J
673 (2012) Mountain ranges favour vigorous Atlantic Meridional Overturning. *Geophysical*
674 *Research Letters* 39(L02705):7 pp., doi:10.1029/2011GL05048

- 675 Sinha B, Topliss B, Blaker AT, Hirschi JJM (2013) A numerical model study of the effects
676 of interannual timescale wave propagation on the predictability of the Atlantic meridional
677 overturning circulation. *Journal of Geophysical Research* Doi:10.1029/2012JC008334
- 678 Sonnewald M, Hirschi JJM, Marsh R (2013) Oceanic dominance of interannual sub-
679 tropical North Atlantic heat content variability. *Ocean Science Discussions* 10:27–53,
680 doi:10.5194/osd-10-27-2013
- 681 Steele M, Morley R, Ermold W (2001) PHC: A global ocean hydrography with a high qual-
682 ity Arctic Ocean. *Journal of Climate* 14:2079–2087
- 683 Taws SL (2013) Seasonal re-emergence of sea surface temperature anomalies in the North
684 Atlantic: An observational and ocean model study. PhD Thesis, University of Southamp-
685 ton p 276pp
- 686 Taws SL, Marsh R, Wells NC, Hirschi JJM (2011) Re-emerging ocean temperature anoma-
687 lies in late-2010 associated with a repeat negative NAO. *Geophysical Research Letters*
688 38(L20601), doi:10.1029/2011GL048978
- 689 Thompson DWJ, Wallace JM (2000) Annular Modes in the Extratropical Circulation. Part
690 I: Month-to-Month Variability. *Journal of Climate* 13:1000–1016
- 691 Timmerman A, Goosse H, Madec G, Fichefet T, Etche C, Dulire V (2005) On the represen-
692 tation of high latitude processes in the ORCA-LIM global coupled sea-ice ocean model.
693 *Ocean Modelling* 8:175–201
- 694 U.S. Department of Commerce (2006) U.S. Department of Commerce, National Oceanic
695 and Atmospheric Administration, National Geophysical Data Center: 2-minute Gridded
696 Global Relief Data (ETOPO2v2). URL [http://www.ngdc.noaa.gov/mgg/global/
697 etopo2.html](http://www.ngdc.noaa.gov/mgg/global/etopo2.html)
- 698 Wallace JM (2000) North Atlantic Oscillation/annular mode: Two paradigms—one phe-
699 nomenon. *Quarterly Journal of the Royal Meteorological Society* 126(564):791–805,
700 doi:10.1002/qj.49712656402
- 701 Zhao J, Johns W (2014) Wind-forced interannual variability of the Atlantic Meridional
702 Overturning Circulation at 26.5N. *Journal of Geophysical Research - Oceans* 119:2403–
703 2419, doi:10.1002/2013JC009407

704 A Decomposition of the AMOC

705 Ocean models typically output the northward velocity for each grid box, which allows us to exactly compute
706 the AMOC (Ψ) in the model, i.e.

$$\Psi(y, z) = \int_z^0 \int_{x_w}^{x_e} v(x, y, z') \, dx dz'. \quad (1)$$

707 In order to make comparisons with the observations taken at 26°N we may also compute components
708 of the transport corresponding to those measured by the 26°N observing array, namely the Florida Straits
709 transport, Ψ_{FST} , the geostrophic (or thermal wind) transport, Ψ_{geo} and the Ekman transport, Ψ_{ekm} .

710 Ψ_{FST} is computed by integrating the meridional velocity, v , through the Florida Straits (between Florida,
711 x_w , and the Bahamas, x_{Bh}), and from the maximum depth of the Florida Straits H_F to the surface,

$$\Psi_{FST} = \int_{H_F}^0 \int_{x_w}^{x_{Bh}} v(x, z') \, dx dz'. \quad (2)$$

712 z' is a dummy integration variable. Ψ_{geo} , the baroclinic geostrophic component arising from zonal density
713 gradients across the Atlantic basin is

$$\Psi_{geo}(z) = \int_z^0 \int_{x_{Bh}}^{x_e} (v_{geo} - \bar{v}_{comp}) \, dx dz', \quad (3)$$

714 where v_{geo} and \bar{v}_{comp} are

$$v_{geo}(x, z) = -\frac{g}{\rho^* f} \int_{-H(x)}^z \frac{\partial \rho}{\partial x} dz' \quad (4)$$

715 and

$$\bar{v}_{comp}(x, z) = \frac{1}{H(x)} \int_{-H(x)}^0 v_{geo}(x, z') dz' + \bar{v}_{FST} \quad (5)$$

716 respectively, x_e is the easternmost extent of the Atlantic (i.e. Africa), $H(x)$ is the maximum depth of the basin
717 as a function of longitude, g being the Earth's gravitational acceleration, ρ the in-situ density, f the Coriolis
718 parameter, and ρ^* a reference density. \bar{v}_{FST} is

$$\bar{v}_{FST} = \frac{\Psi_{FST}}{A} \quad (6)$$

719 with A being the cross-sectional area of the Atlantic basin east of the Bahamas.

720 We define Ψ_{ekm} , the Ekman (wind driven) component, here as a function of latitude and depth compen-
721 sated by a section mean return flow to ensure no net transport,

$$\Psi_{ekm}(y, z) = \int_{-H_{max}(y)}^z \int_{x_w}^{x_e} (v_{ekm} - \bar{v}_{ekm}) dx dz', \quad (7)$$

722 where v_{ekm} and \bar{v}_{ekm} are

$$v_{ekm} = -\frac{1}{(\rho^* f L \Delta_z)} \int_{x_w}^{x_e} \tau_x dx \quad (8)$$

723 and

$$\bar{v}_{ekm} = -\frac{1}{(\rho^* f A)} \int_{x_w}^{x_e} \tau_x dx \quad (9)$$

724 respectively, L being the basin width, Δ_z the Ekman depth, and $H_{max}(y)$ the latitudinally dependent max-
725 imum depth of the basin. The Ekman depth, Δ_z , which defines the base of the Ekman layer in which the
726 wind driven transport occurs we chose to be 100 m. The choice of Δ_z does not strongly affect the resulting
727 overturning profile. Note that the compensation term associated with the Ekman transport could equally be
728 added to \bar{v}_{comp} , but that it will be small compared with the other terms.

729 Therefore at 26.5°N the AMOC transport can be considered as the sum of these components plus a
730 residual term, Ψ_{res} ,

$$\Psi = \Psi_{FST} + \Psi_{geo} + \Psi_{ekm} + \Psi_{res}. \quad (10)$$

731 where Ψ_{res} can be obtained by rearranging Eq. (10). If averaged over a time longer than a few cycles
732 of the local inertial period the residual term is small (order 1 Sv), and can be ignored. It should be noted,
733 however, that this term can dominate the AMOC variability at near-inertial time scales (Blaker et al, 2012;
734 Sevellec et al, 2014).